ОБЪЕДИНЕННЫЙ
ИНСТИТУТ
ЯДЕРНЫХ
ИССЛЕДОВАНИЙ
ДУБНА

E1 - 7552

N.N.Govorun, I.M.Ivanchenko, S.S.Kirilov, R.Leiste,
A.A.Nomofilov, N.M.Piskunov, V.I.Sharov,
I.M.Sitnik, E.A.Strokovsky, L.N.Strunov,
G.G.Vorobyov

INTERFERENCE MEASUREMENTS OF THE REAL PART OF THE $\pi^- p$ FORWARD ELASTIC SCATTERING AMPLITUDE AT 2.44 AND 1.91 GeV/c

1973

ЛАБОРАТОРИЯ ВЫСОКИХ ЭНЕРГИЙ

E1 - 7552

N.N.Govorun, I.M.Ivanchenko, S.S.Kirilov, R.Leiste, A.A.Nomofilov, N.M.Piskunov, V.I.Sharov, I.M.Sitnik, E.A.Strokovsky, L.N.Strunov, G.G.Vorobyov

INTERFERENCE MEASUREMENTS OF THE REAL PART OF THE $\pi^- p$ FORWARD ELASTIC SCATTERING AMPLITUDE AT 2.44 AND 1.91 GeV/c

Submitted *to ЯФ*

Говорун Н.Н., Иванченко И.М.,
Кирилов С.С. и др.

E1 - 7552

Интерференционные измерения вещественной части амплитуды упругого рассеяния вперед при импульсах 2,44 и 1,91 Гэв/с

С помощью созданного в ЛВЭ ОИЯИ магнитного искрового спектрометра измерено дифференциальное сечение π^-p -рассеяния в области кулоновской интерференции, что позволило вычислить вещественную часть амплитуды π^-p -рассеяния вперед.

Препринт Объединенного института ядерных исследований.
Дубна, 1973

Govorun N.N., Ivanchenko I.M.,
Kirilov S.S. et al.

E1 - 7552

Interference Measurements of the Real Part of the π^-p Forward Elastic Scattering Amplitude at 2.44 and 1.91 GeV/c

The results of measurements of the real part of the π^-p forward elastic scattering hadron amplitude at 2.44 and 1.91 GeV/c are presented. The measurements have been made by detecting the scattered particle using wire spark chambers in the range $0.5\cdot10^{-3} \leq t \leq 5\cdot10^{-3}$ GeV^2/c^2. The present data, that are insignificantly different from the preliminary ones reported earlier, are compared with theoretical predictions. The experimental procedure and the analysis of the experimental data are described in detail.

**Preprint. Joint Institute for Nuclear Research.
Dubna, 1973**

1. Introduction

This paper as well as a number of other papers [1-5] is devoted to an investigation of π^-p elastic scattering in the Coulomb interference region ($0.5\cdot10^{-3} \leq t \leq 5\cdot10$ GeV^2/c^2) at energies of several GeV. As is known, an analysis of the interference picture in the differential cross section makes it possible to determine the value and sign of the ratio $\alpha(E,t) \underset{t\to 0}{=} \mathrm{Re}\,A_n / \mathrm{Im}\,A_n$ between the real and imaginary parts of the hadron amplitude.

A measurement of the real part of the πp forward elastic scattering amplitude at 3-6 GeV (Dubna) [1-4] and 8-26 GeV (Brookhaven) [6] proves the validity of the dispersion relations at energies of the order of several GeV. The results of our measurements at 1.91 and 2.44 GeV are interesting because at energies of 1-3 GeV the behaviour of the total cross section $\sigma_{\pi p}(E)$ is determined to a large extent by resonances in the πp system. Inconsistency of the experimental data on $\mathrm{Re}\,A_n$ with the dispersion-relation calculations [7] could indicate the existence of unknown resonances in this energy range since the structure of the dispersion integral is such that the value of $\mathrm{Re}\,A_n(E_0)$ is sensitive to the behaviour of $\mathrm{Im}\,A_n(E) = k\,\sigma_{tot}(E)/4\pi$ in the whole region of E values close to E_0. For example, paper [8] indicates that new resonances may exist at energies of 1-3 GeV. The results of our measurements contradict these assumptions.

In this paper much attention is focused on the methods of experimental data analysis because it is necessary to throw light on a number of specific problems (for example, inadditivity of measurements in target-full and target-

empty runs) arising when the measured angles are not sufficiently large in comparison with the average angle of multiple scattering.

The experimental setup described in this paper is somewhat different from that used earlier in experiments at $E > 3$ GeV[1]. The necessity to increase the aperture of the device with decreasing the primary beam energy causes main modifications (base decrease and trigger change).

2. Apparatus

The experimental setup used on-line with the BESM-4 computer consists of a beam transport system, liquid hydrogen target, magnetic spark chamber spectrometer, system of scintillation counters and fast electronics operating as a monitor and trigger. The experimental layout is shown in fig. 1.

The monitor $S_1S_2S_3$ was used for determining a flux of pions at the target. Scattering events were selected by the trigger $S_1 S_2 S_3 S_5$. The size of the counter S_5 and the hole diameter in its centre were chosen so that the spark chambers might be triggered at scattering angles of 10-35 mrad. At $p \simeq 2$-2.5 GeV/c this corresponded to the range $-t \simeq p^2\theta^2 \sim 0.5\text{-}5 \cdot 10^{-3}$ (GeV/c)^2. At these energies such a simple selection system was rather effective, the trigger suppression factor of the unscattered beam was equal to ~ 10.

The magnetic spectrometer involves spark chambers with magnetostrictive readout and an analyzing magnet. The spark chambers SC1-SC7 (200 x 200 mm^2) were used for determining the scattering angle of particles. The information from the chambers SC4-SC9 was used for a momentum analysis. The chambers SC8, SC9 (480 x 480 mm) were located behind the analyzing magnet. The detailed characteristics of the spark chambers and data link are presented in ref.[1]. In order to reduce multiple scattering, the space between the chambers was filled with gasiform helium. The scattering angle was determined with an accuracy of $\delta\theta = 0.6$ mrad for 2.44 GeV/c and $\delta\theta = 0.8$ mrad for 1.91 GeV/c, the momentum width with a relative accuracy of $\delta p/p \simeq 0.35\%$.

The 50 cm hydrogen target used in the experiment is described in detail in ref.[9]. The isolation of the target walls from the surroundings by the vacuum sleeves ($L \simeq 60$ cm) enabled us to identify scattering events on hydrogen and background ones by the z-coordinate of the interaction point (see fig. 2).

The average momentum p_0 and the beam composition were determined in special runs. The value of p_0 was measured with an accuracy of better than 0.5%. Figure 3 shows the identification of different particles by means of a threshold Čherenkov spectrometer. The contamination of muons and electrons in the beams fraction satisfying the condition $|p - p_0|/p_0 \leq 0.025$ was equal to 9% at 2.44 GeV/c and 10% at 1.91 GeV/c (see fig. 4).

3. Exposure

All the operation time was divided into sequential runs. One tape of the computer corresponded to each of them. Apart from the procedure of data taking, each run included all additional measurements necessary for data processing. As a result of this, each tape was an independent source of information for determining the differential cross sections. Experimental conditions and apparatus operation were continuously controlled by means of the computer. The measurements were carried out as follows.

1. Target-empty exposure
   a) without selective trigger (trigger of the spark chambers from the monitor);
   b) in the operating mode (trigger of the spark chambers from $S_1 S_2 S_3 S_5$ coincidences).
2. Exposure of a 3 cm thick lead plate located near the target (trigger of the spark chambers from the monitor, the transferred event is marked if $S_1 S_2 S_3 S_5$ coincidence takes place).

3. Target-full exposure
   a) without selective trigger;
   b) in the operating mode.

The information obtained in exposures 1a and 3a was used to determine the angular resolution of the spectrometer and the average deviation angle of unscattered pions in the analyzing magnet. The data from exposure 2 together with those from exposures 1a and 3a were used to define the geometrical efficiency of the device. In exposure 1b the events were accumulated to measure the background, the main source of which were the target walls.

4. Data Processing

The data analysis has been carried out in three steps. Using the program of the first stage the geometrical reconstruction of the events was performed. At the second stage the πp elastic scattering distribution was obtained as a function of the square of the four-momentum transfer. The real part of the nuclear forward elastic scattering amplitude was determined at the third stage.

4.1. The program of the first stage contains the following selection criteria.

a) A set of effectively operating chambers makes it possible to determine the trajectories of the particle before and after the target and to measure its deflection angle in the magnet. The chamber is considered to be effective if there is one and only one spark in the chamber.

b) The particle trajectories before and after the target are matched, i.e., the distance between the corresponding straight lines in space is less than the particular value (0.5 cm).

c) The y -coordinates of the sparks in the chambers SC4-SC9 lie well on the straight line.

The data on the events satisfying the above selection criteria (scattering and deviation angles in the magnet, coordinates of the interaction point) were put on the secondary tape.

4.2. At the second stage the events were identified

according to the z -coordinate criterion of the interaction point $|z-z_0| \leq 55$ cm (z_0 is the target centre) and the "elasticity" criterion $|p-p_0|/p_0 \leq 0.025$. The limiting constants were based on the distributions presented in figs. 2 and 5. The identified events were grouped according to $t_{i-1} \leq |t| < t_i$ intervals. The t-distribution of scattering events in the target-empty exposure was modified by imitating the influence of the multiple scattering on hydrogen since this effect takes place in the target-full exposure. In the region of minimal $|t|$ the modified distribution exceeded the real one by $\simeq 12\%$.

The elastic cross section for each $t_{i-1} \leq t < t_i$ interval has been determined from the formula

$$\sigma_i = \frac{1}{n}\left(\frac{N_{fi}}{M_f} - \frac{N_{ei}}{M_e}\right). \qquad (1)$$

Here N_{fi}, N_{ei} are the numbers of elastic scattering events in the $t_{i-1} \leq t < t_i$ interval for the full and empty targets, respectively; n is the number of nuclei per cm^2 in the target; M_f, M_e are the effective monitor numbers for the full and empty targets determined as

$$M = m \cdot \epsilon \cdot \eta \cdot \rho. \qquad (2)$$

Here m is the monitor number; ϵ is the detection efficiency of the elastic scattering events; η is the coefficient of the beam attenuation in the target matter being equal to $\exp(-\sigma_{tot} \cdot n)$ where σ_{tot} is the $\pi^- p$ total cross section (for the empty target $\eta = 1$). The coefficient ρ was introduced to take into account the losses of events due to pion decays and interactions along the particle trajectory inside the installation and also the losses due to the application of the "elasticity" criterion. Its value was measured with an error of less than 1% using the experimental data (exposure 1a).

The efficiency $\epsilon = n_1/n_2$ was calculated on the set of test events corresponding to the propagation of a single particle through all the chambers of the spectrometer;

n_1 is the number of events satisfying the criteria of the first stage program; n_2 is the total number of test events. The test events were selected by $S_1S_2S_3S_4$ coincidences with sufficient confidence (the counter S_4 was located behind the magnet, its size insignificantly exceeded the hole diameter in the counter S_5). Under all operation conditions the events transferred to the computer were marked if $S_1S_2S_3S_4$ coincidence took place. A large fraction of these events in the accepted information (~ 25% - operating mode and ~ 90% - trigger from the monitor) made it possible to calculate the ϵ value (~ 65%) with a good statistical accuracy ($\Delta\epsilon/\epsilon \simeq 0.5\%$). Simultaneous storage of the operating and control data enabled us to avoid the shift in the estimated value of σ_i that could appear due to efficiency drift in the exposure.

The geometrical efficiency of the device was dependent on the dimensions of the spark chambers and counter S_5*. The efficiency as a function of the scattering angle of the particle and its deviation angle in the magnet was calculated by the Monte-Carlo method. The input data (coordinate-angular distribution of the input beam, boundaries of the spark chambers, hole coordinated of the counter S_5 in the system of spark chambers) were obtained in exposures 1a, 2, 3a. The inverse geometrical efficiency determined the weight of the events when plotting the t -distribution. The averaged value of the geometrical efficiency for each $t_{i-1} \le t < t_i$ interval are presented in Table I.

The statistical errors $\Delta\sigma_i$ in σ_i were determined mainly by the statistics collected in the operating mode of the exposure. The statistical error of the background made practically no contribution to the total error since its value in comparison with the measured effect did not

---

*The homogeneity of the spark chamber efficiency was measured with an error of 1% /1/. The efficiency of the counter S_5 was also homogeneous and equal to 99.7%.

Table I The σ_i elastic cross sections at 2.44 and 1.91 GeV/c (without corrections for the multiple scattering effects, apparatus resolution and muon and electron contamination in the beam). The averaged geometrical efficiency $\bar{\gamma}$ for each $t_{i-1} - t_i$ interval.

i	p = 2.44 GeV/c			p = 1.91 GeV/c		
	$t_{i-1} \div t_i$ (GeV^2/c^2 · 10^{-3})	σ_i (mb)	$\bar{\gamma}$	$t_{i-1} \div t_i$ (GeV^2/c^2·10^{-3})	σ_i (mb)	$\bar{\gamma}$
I	0,590÷0,850	0,150±0,005	0,74	0,564÷0,759	0,135±0,005	0,89
2	0,850÷1,157	0,090±0,004	0,90	0,759÷0,983	0,092±0,004	0,96
3	1,157÷1,511	0,060±0,003	0,96	0,983÷1,235	0,069±0,003	0,98
4	1,511÷1,913	0,051±0,003	0,98	1,235÷1,517	0,055±0,003	0,96
5	1,913÷2,361	0,041±0,003	0,97	1,517÷1,827	0,041±0,003	0,92
6	2,361÷2,857	0,034±0,002	0,96	1,827÷2,166	0,042±0,003	0,87
7	2,857÷3,401	0,034±0,002	0,90	2,166÷2,535	0,037±0,003	0,80
8	3,401÷3,991	0,038±0,002	0,83	2,535÷2,932	0,031±0,003	0,72
9	3,991÷4,629	0,037±0,003	0,70	2,932÷3,358	0,030±0,003	0,63

exceed 5 % (see fig. 5). The background was strongly depressed due to a good selection of interactions on hydrogen by the z-coordinate of the interaction point and a good momentum resolution of the device permitting the separation of the elastic scattering effect from that of $\pi-\mu$ decays (see the enhancement in the momentum distribution on the left of the elastic peak in fig. 5a). As is seen from fig. 5b which presents the momentum distribution for one of the scattering angle intervals larger than the limiting one in the $\pi-\mu$ decay, inelastic processes did not contribute to the elastic peak. A small asymmetry of the elastic peak is related to the asymmetry of the beam momentum distribution (see fig. 4).

4.3 When determining the real part of the $\pi^- p$ elastic scattering amplitude the differential cross section in the region of small t was described by the Bethe formula /10,11,12/

$$f(t,\alpha)=\left(\frac{d\sigma}{dt}\right)=[A_c(t)\exp(i\delta)+A_n(t,\alpha)]^2, \qquad (3)$$

where

$$A_n(t,\alpha)=\frac{\sigma_{tot}}{4\sqrt{\pi}}(\alpha+i)\sqrt{F} \qquad (4)$$

is the strong interaction amplitude,

$$A_c(t)=\frac{2\sqrt{\pi}}{137|t|}\sqrt{F} \qquad (5)$$

is the Coulomb interaction amplitude
and

$$\delta=\frac{1}{137}\left[\ln\frac{t_0}{|t|}-0{,}577\ldots\right] \qquad (6)$$

is the phase shift between the amplitudes A_c and A_n. The form factor was taken in the form

$$F=\exp(Bt). \qquad (7)$$

The spin-flip amplitude in eq. (4) was neglected because it was very small /13/. The fitted parameter was $\alpha = \mathrm{Re}A_n/\mathrm{Im}A_n$. The value of t_0 (0.11 GeV^2/c^2) was taken from ref. /12/; the values of σ_{tot} (34.1 mb at 2.44 GeV/c and 35.9 mb at 1.91 GeV/c) from ref. /14/; the slope parameter B (8 $GeV^{-2}\cdot c^2$) from ref. /15/.

The t-distributions of the scattering events obtained from the experiment are not quite adequate the differential cross section. In the region of the least transfers they are determined to a great extent by the multiple scattering effects on hydrogen and apparatus errors in measuring the scattering angle (the error in determining the momentum was negligible so its influence can be neglected). In view of this, to approximate the experimental data, instead of function (3) we used the function

$$g(t,\alpha)=\int_{t-\tau}^{t+\tau} f(t',\alpha)\,W(t',t)\,dt' \qquad (8)$$

describing the interaction taking into account the above-mentioned effects. The kernel of transformation (8) takes the form

$$W(t',t)=\frac{1}{2p_0^2\sigma_f^2}\exp\left[-\frac{(\sqrt{t}-\sqrt{t'})^2}{2p_0^2\sigma_f^2}\right]\exp\left(-\frac{\sqrt{tt'}}{p_0^2\sigma_f^2}\right)I_0\left(\frac{\sqrt{tt'}}{p_0^2\sigma_f^2}\right), \qquad (9)$$

where I_0 is the Bessel function of the imaginary argument, p_0 is the beam momentum. The value of σ_f in eq. (9) was determined as a parameter of the Releigh distribution

$$V(\theta,\sigma_f)=\frac{\theta}{\sigma_f^2}\exp\left(-\frac{\theta^2}{2\sigma_f^2}\right) \qquad (10)$$

approximating the experimental angular distribution near zero scattering angle obtained in the target-full exposure (see figs. 6,7)*. At the lower boundary of the region

---

* Simultaneous treatment of the multiple scattering and apparatus resolution by means of eq. (8) is correct if the lower limit of the region of the studied angles is large enough in comparison with the value of σ_f. In our case this condition was fulfilled - the scattering angles $\theta \geq 8\,\sigma_f$ were considered.

$0.0006 \leq t \leq 0.005$ (GeV/c)^2 the function $g(t,\alpha)$ exceeds the function $f(t,\alpha)$ by ~15%. At the upper boundary they practically coincide. These functions are shown in fig. 8 at the same values of the parameter α. Taking into account the multiple scattering effects and apparatus error in the angle measurements it is possible to avoid a significant shift in estimating the parameter α (in our case this difference was $\Delta\alpha \simeq 0.06$).

The parameter α was estimated from the minimum of the functional

$$M(\alpha) = \sum_i \left[\frac{G_i(\alpha) - \sigma_i}{\Delta\sigma_i}\right]^2, \qquad (11)$$

where

$$G_i(\alpha) = \int_{t_{i-1}}^{t_i} g(t,\alpha)\,dt \qquad (12)$$

and σ_i, $\Delta\sigma_i$, t_i was determined in §4.2.

5. Results and Discussion

Table I presents the results of measurements of the elastic cross sections σ_i for $t_{i-1} \leq |t| < t_i$ intervals at 2.44 and 1.91 GeV/c. Corrections for multiple scattering and apparatus resolution are absent in the value of σ_i because when calculating the value of α it was more correct to modify the theoretical curve approximating the experimental data (see § 4.3).

Figures 8 and 9 show the differential cross sections $d\sigma/dt = \sigma_i/(t_i - t_{i-1})$ and the theoretical curves (8) with the parameters α found by the least-square fit.

The influence of different experimental errors on the eror in α is shown in Table II. A possible inaccuracy in α related to the calculation uncertainty of the phase shift δ from eq. (3) is estimated as $|\Delta\alpha| < 0.015$ [12]. To measure differential cross sections, a narrow t-interval close to 0 is chosen, therefore the estimate α is

Table II

Influence of various errors on the error in α.

k	Error source	$(\Delta\alpha)_k$
1	Statistical error	0.023
2	Normalization error $\Delta q/q \simeq \pm 1\%$	0.014
3	Uncertainty in the beam composition $n(e+\mu)/n(\pi+e+\mu) \simeq \pm 1\%$	0.005
4	Error in determining the average momentum of the beam $\Delta p_0/p_0 \simeq \pm 0.5\%$	0.005
5	Correction inaccuracy for multiple scattering	0.003
6	Error in the total cross section $\Delta\sigma_{tot} \simeq \pm 0.5$ mb	0.012
7	Error in the slope parameter $B \simeq \pm 1$ GeV$^{-2}\cdot c^2$	0.002
	Summary error $\Delta\alpha = \sqrt{\sum_k (\Delta\alpha)_k^2}$	0.03

weakly sensitive to assumptions about the t-dependence of A_n in eq. (4) [16] and to the form factor in A_c.

The values of α obtained at 2-6 GeV/c in this paper and in refs. [1-4,16] are presented in Table III and fig. 10 which also present the results obtained at 8-26 GeV/c in Brookhaven [6]. The solid curve in fig. 10 has been calculated by Höhler and Strauss using dispersion relations [7]. The Serpukhov data on the total cross sections used in ref. [7] do not change practically the predictions for $\mathrm{Re}\,A_n(E)$ in our energy range obtained in the

previous calculation [17] despite the fact that they (the Serpukhov data) have changed earlier assumptions about the asymptotic behaviour of the total cross sections. This fact points out that at energies of several GeV $Re A_n(E)$ is weakly sensitive to the total cross-section behaviour at energies higher 30 GeV. The dashed line in fig. 10 has been calculated by Minami and Sasaki [8]. To describe π p interactions, in this calculation the modified interference model was used successfully explaining the peak structure in the energy dependence of the π p backward elastic scattering differential cross sections and the behaviour of π^+p total cross section. For satisfactory description of the data on the π^-p total cross sections the authors assumed that there existed a new parity doublet of isobars (M = 2.3 GeV, Γ = 0.2 GeV, T=1/2). As is seen from fig. 10, the predictions for $Re A_n(E)$ resulting from here contradict the data of our experiment. These data are in good agreement with the dispersion-relation calculation [7]. This makes it possible to conclude that in the region of the πp resonance behaviour the set of total cross section data is sufficient in order that the interpolation procedure used in ref. [7] may be correct to describe the energy dependence $\sigma_{tot}(E)$.

In conclusion the authors would like to express their gratitude to the operational divisions and to the synchrophasotron division of the Laboratory of High Energies of JINR for good operation of the accelerator and electrophysical equipment. We thank V.A.Voblikov, S.A.Dolgij, A.V.Karpunin, Yu.V.Kulikov, A.G.Muryzin, Yu.I.Salomatin for their help in preparing the measuring equipment and also to L.N. Barabash, R.N.Kaplina, Z.P. Motina, L.A.Rachkova for their technical assistance in data processing.

We express our acknowledgement to A.M.Baldin, Corresponding Member of the Academy of Sciences of USSR and to the Directorate of the Laboratory of High Energies for their support of this experiment.

Table III

The values of $\alpha = Re A_n / Im A_n$ for the π^-p elastic scattering amplitude obtained in this and previous papers of our group.

p (GeV/c)	$\alpha \pm \Delta\alpha$	χ^2	Number of experimental dots	Refs.
1,91	-0,07±0,03	5,5	9	this paper
2,44	-0,17±0,03	5,9	9	this paper
3,06	-0,17±0,05	4,8	7	/1/
3,48	-0,17±0,07	2,6	7	/16/
4,17	-0,15±0,05	1,1	5	/3,4/
4,56	-0,16±0,04	7,6	7	/1/
4,95	-0,14±0,04	4,5	6	/3,4/
5,65	-0,12±0,04	7,1	5	/3,4/
6,13	-0,22±0,09	3,5	7	/16/

References

1. G.G.Vorobyov, N.N.Govorun, I.A.Golutvin, Yu.V.Zanevsky, I.M.Ivanchenko, S.S.Kirilov, Yu.T.Kiryushin, D.Kiselewska, E.V.Lazutin, R.Leiste, T.S.Nigmanov, B.Niczyporuk, A.A.Nomofilov, N.M.Piskunov, V.P.Pugachevich, V.D.Ryabtsov, I.M.Sitnik, D.A.Smolin, L.N.Strunov, E.N.Tsyganov. JINR Preprint, P1-4445, Dubna, 1969.
2. I.M.Ivanchenko, I.A.Golutvin, N.N.Govorun, S.S.Kirilov, Yu.T.Kiryushin, D Kiselewska, E V.Lazutin, R.Leiste, B Niczyporuk, T.Y.Nigmanov, A.A.Nomofilov, N.M.Piskunov, V.P.Pugachevich, V.S.Ryabtsov, I.M.Sitnik, D.A.Smolin, L.N.Strunov, E.N.Tsyganov, G.G.Vorobyov, Yu.V.Zanevsky. Report no.411 at the Lund Intern.Conf. on Elem. Particles (1969). See rapporteur's talk Dilella p. 151-153 in Proc. of the Lund Intern. Conf. on Elem. Particles, Editor G. von Dardel (1969).
3. N.N.Govorun, I.M.Ivanchenko, S.S.Kirilov, R.Leiste, A.A.Nomofilov, N.M.Piskunov, I.M.Sitnik, V.I.Sharov, L.N.Strunov, G.G.Vorobyov. Report no. 1a-19 XVth Intern. Conf. on High Energy Phys. (Kiev, 1970). See rapporteur's talk J.Allaby p. 15 in Proc. of the XVth Intern. Conf. on High Energy Phys. (Naukova Dumka, Kiev, 1972).
4. A.A.Nomofilov, I.M.Sitnik, L.N.Strunov. Intern. Seminar on Binary Reactions of Hadrons at High Energies, p. 192 (Dubna, 1971).
5. G.G.Vorobyov, M.F.Likhachev, A.A.Nomofilov, N.M.Piskunov, I.M.Sitnik, L.N.Strunov, V.I.Sharov. Intern. Conf. on Instrumentation in High Energy Phys., v. 1, p. 66 (Dubna, 1971).
6. K.J.Foley, R.S.Jones, S.J.Lindenbaum, W.A.Love, S.Ozaki, E.D.Platner, C.A.Quarles and E.H.Willen. Phys.Rev., 181, 1775 (1969).
7. G.Höhler and R.Strauss. Preprint Univ. of Karlsruhe (1970).
8. S.Minami and K.Sasaki. Prog. Theor. Phys., 42, 275 (1969).
9. L.B.Golovanov. Elem.Particles and Atomic Nuclei, 2, 717 (Moscow, Atomizdat, 1972).
10. H.A.Bethe. Ann.Phys., 3, 190 (1958).
11. M.P.Locher. Nucl.Phys., B2, 525 (1967).
12. G.B.West and D.R.Yennie. Phys.Rev., 172, 1413(1968).
13. a) A.De Lesquen, B.Amblard, R.Beurtey, G.Cozzika, J.Bystricky, J.Deregel, Y.Ducros, J.M.Fontain, A.Gaidot, M.Hansroul, F.Lehar, J.P.Merlo, S.Miyashita, J.Movchet, L. van Rossum. Phys.Lett., 40B, 277 (1972).
    b) G.Cozzika, Y.Ducros, A.Gaidot, A. De Lesquen, J.P.Merlo, L. van Rossum. Phys.Lett., 40B, 281 (1972).
14. A.A.Carter, K.F.Riley, R.J.Tapper, D.V.Bugg, R.S.Gilmore, K.M.Knight, D.C.Salter, G.H.Stafford, E.J.N.Wilson - J.D Davies, J.D.Dowell, P.M.Hattersley, R.J.Homer, A.W.O'Dell. Phys.Rev., 172, 1413 (1968).
15. T.Lasinski, R.Levi Setti, B.Schwarzschild, P.Ukleja. Nucl.Phys., B37, 1 (1972).
16. A.A.Nomofilov, I.M.Sitnik, L.A.Slepets, L.N.Strunov, L.S.Zolin. Phys.Lett., 22, 350 (1966); Letters to JETP, 6, 546 (1967).
17. G.Hohler, G.Ebel. J.Giesecke. Zeitschrift für Phys., 180, 430 (1964).

Received by Publishing Department
on November 14, 1973.

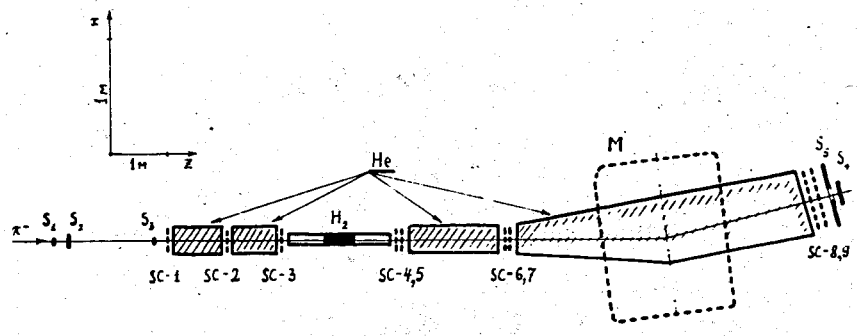

Fig. 1. Experimental layout in the π^--meson beam at the Dubna synchrophasotron. S_1-S_5. scintillation counters; SC1–SC9. wire spark chambers; H_2.liquid hydrogen target with vacuum sleeves; M. analyzing magnet; He . ionguide filled with helium.

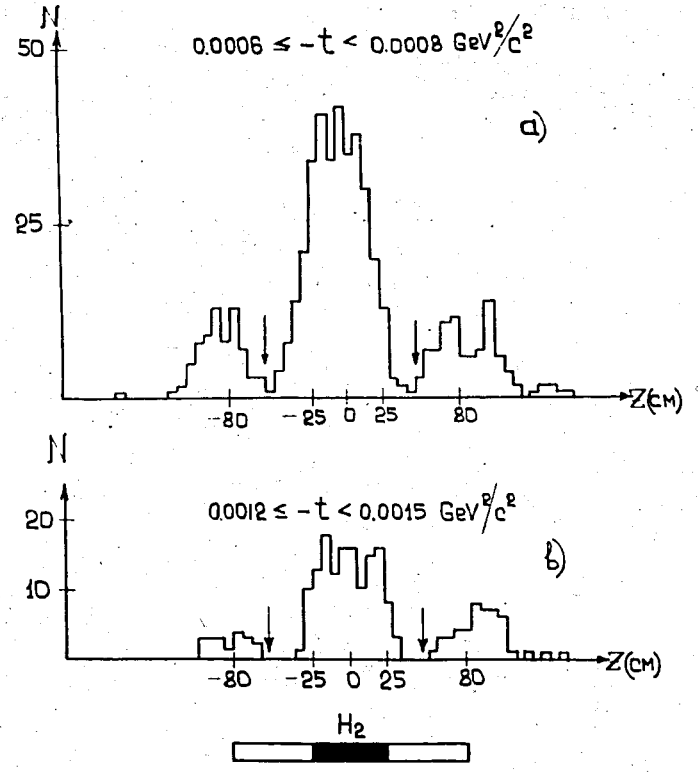

Fig. 2. z - coordinate distribution of elastic scattering events for two intervals of the momentum transfer squared. The vertical arrows show the limits within which the events were considered as scattered on hydrogen.

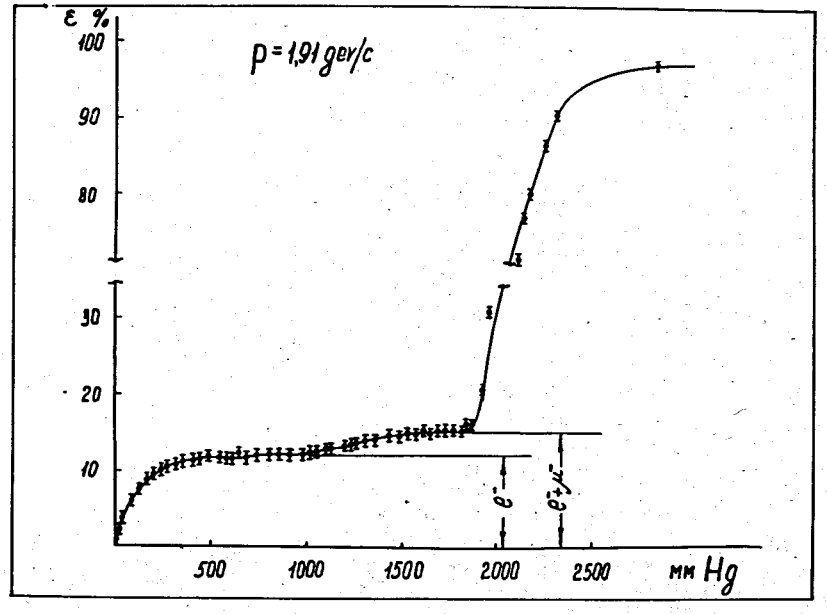

Fig. 3. Identification of electrons, muons and pions by means of the threshold Cherenkov counter (counting rate dependence on the propane pressure).

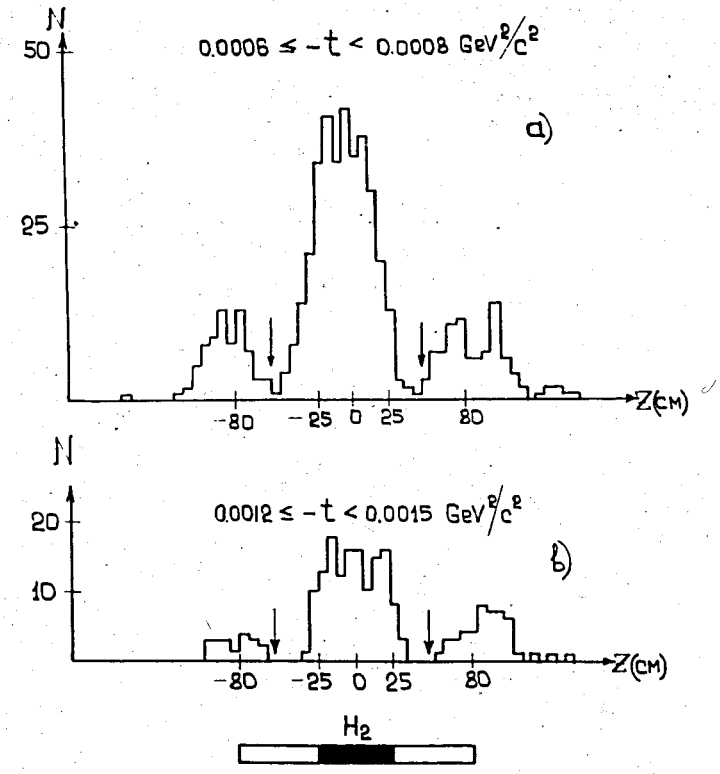

Fig. 2. z - coordinate distribution of elastic scattering events for two intervals of the momentum transfer squared. The vertical arrows show the limits within which the events were considered as scattered on hydrogen.

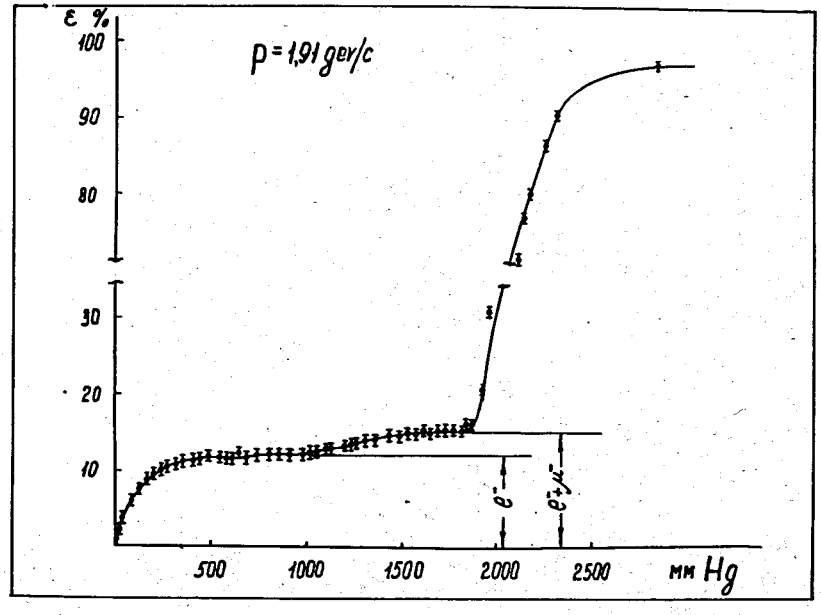

Fig. 3. Identification of electrons, muons and pions by means of the threshold Čherenkov counter (counting rate dependence on the propane pressure).

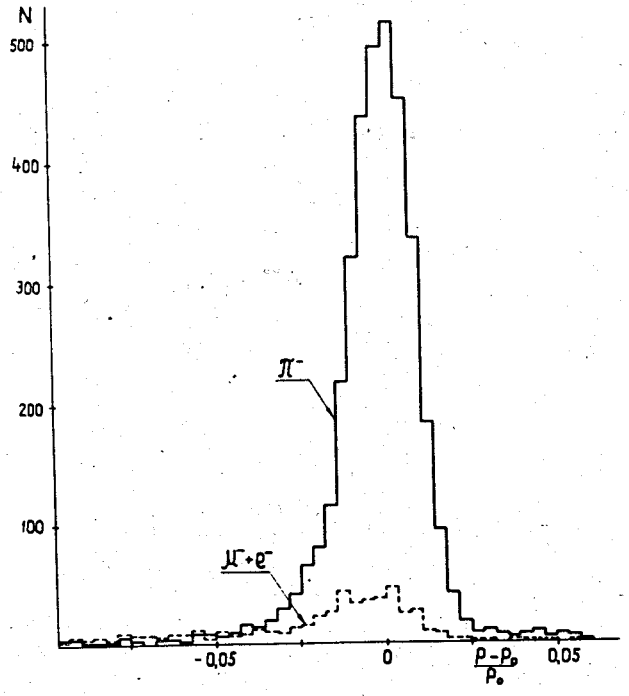

Fig. 4. Momentum distribution of pions, muons and electrons in the unscattered beam.

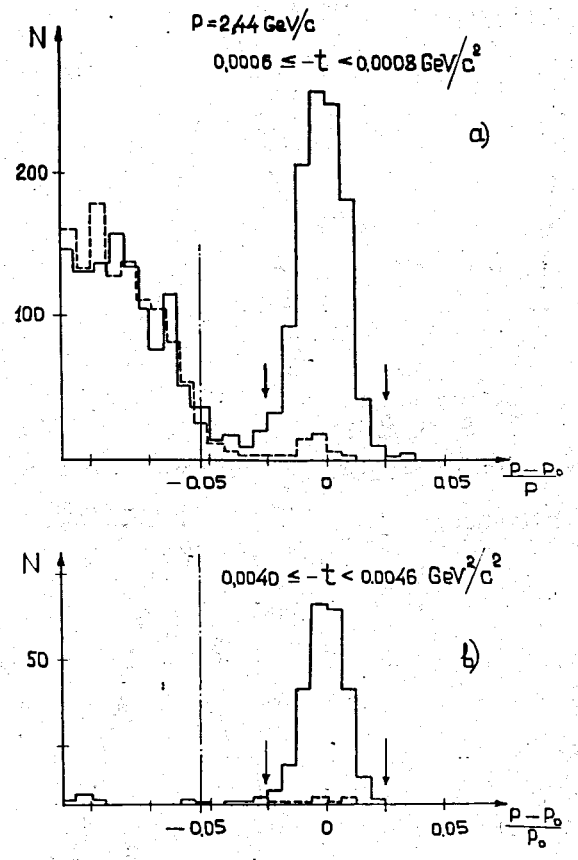

Fig. 5. Momentum distribution of the scattering events satisfying the z-criterion for two intervals of the momentum transfer squared. Solid line - full target, dashed line - reduced background of the empty target. The vertical arrows indicate the limits within which the events were considered to be elastic. The kinematic region of the πp inelastic interaction is on the left of the vertical dash-dotted curve. The enhancement on the left of the elastic peak is due to $\pi - \mu$ decays.

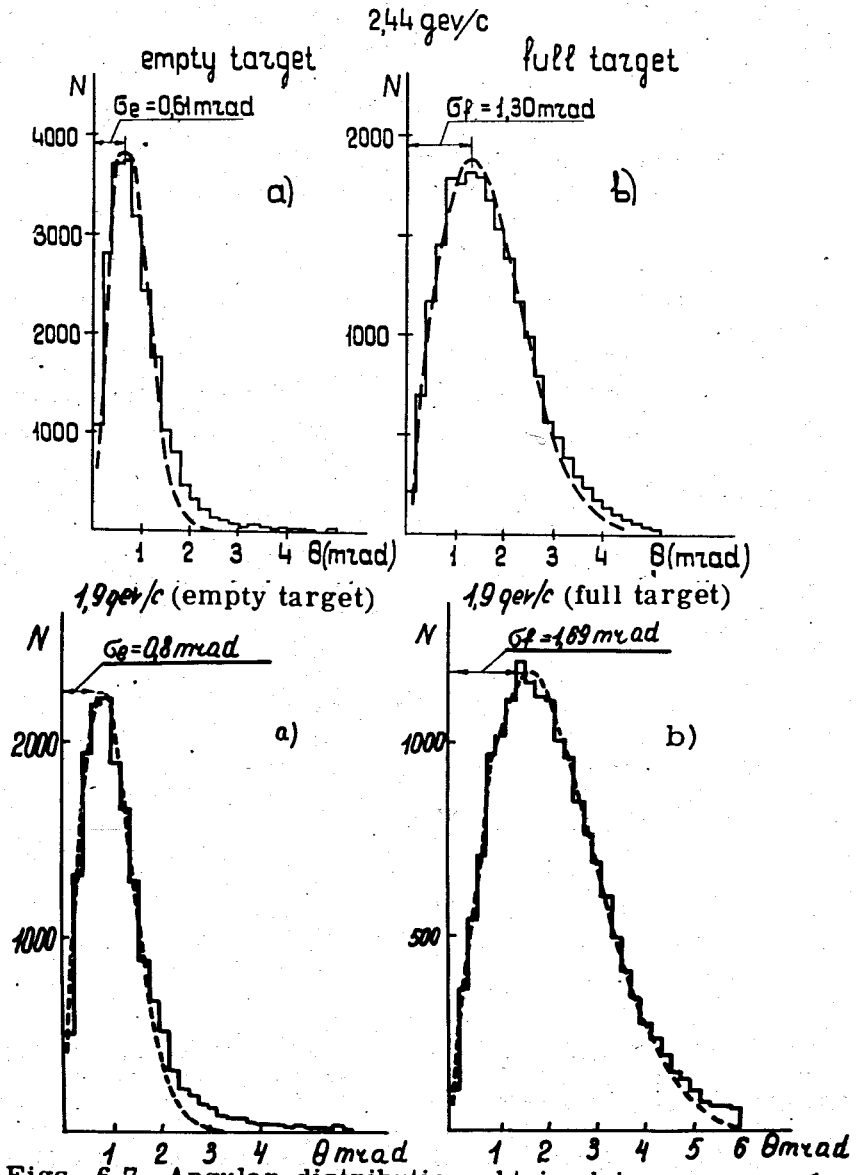

Figs. 6,7. Angular distribution obtained in exposures 1a and 3a (without selective trigger) from which the parameters σ_e and σ_f were determined characterizing the angular resolution of the apparatus and multiple scattering in the target.

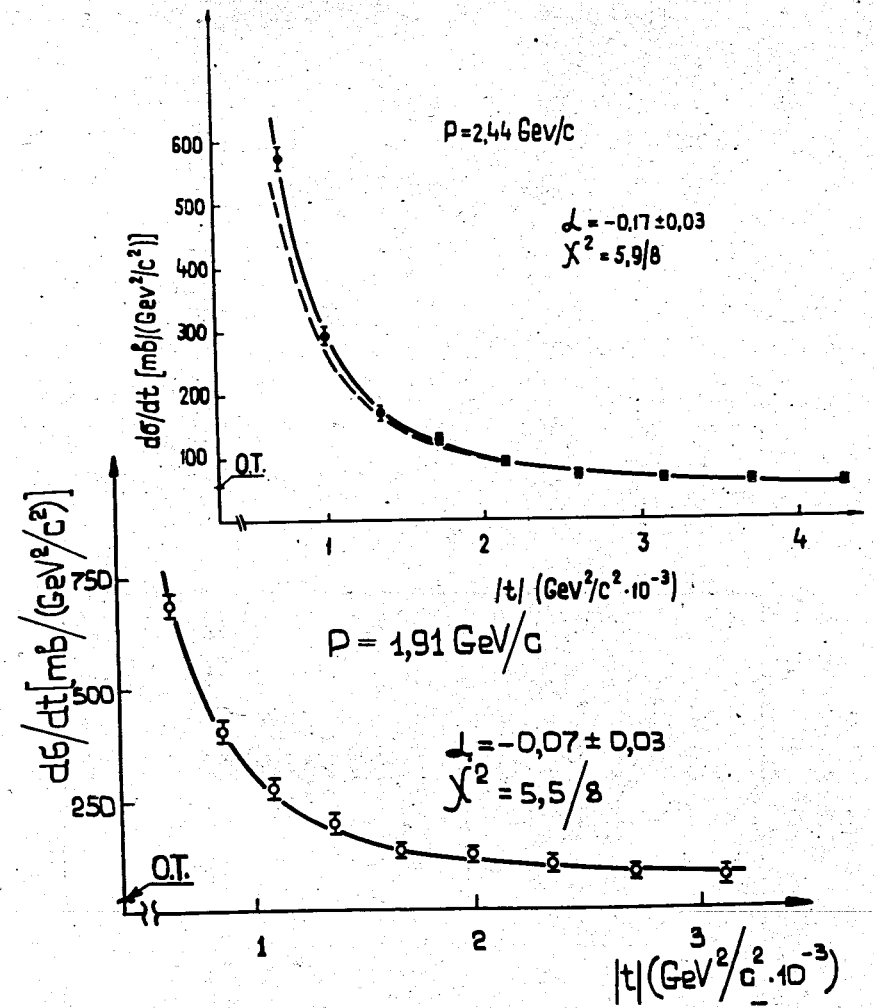

Fig. 8,9. Differential cross sections $d\sigma/dt(\bar{t}_i)$ at 2.44 and 1.91 GeV/c; $d\sigma/dt = \sigma_i/(t_i - t_{i-1})$, $\bar{t}_i = \frac{t_i + t_{i-1}}{2}$.

The solid curves are drawn through the points

$$\frac{dG}{dt}(\bar{t}_i) = \frac{1}{t_i - t_{i-1}} \int_{t_{i-1}}^{t_i} g(t,\alpha)\,dt,$$

where $g(t, \alpha)$ is the transformed Bethe function. In fig. 8 the dashed line is the Bethe curve without unfolding the multiple scattering and final apparatus resolution effects.

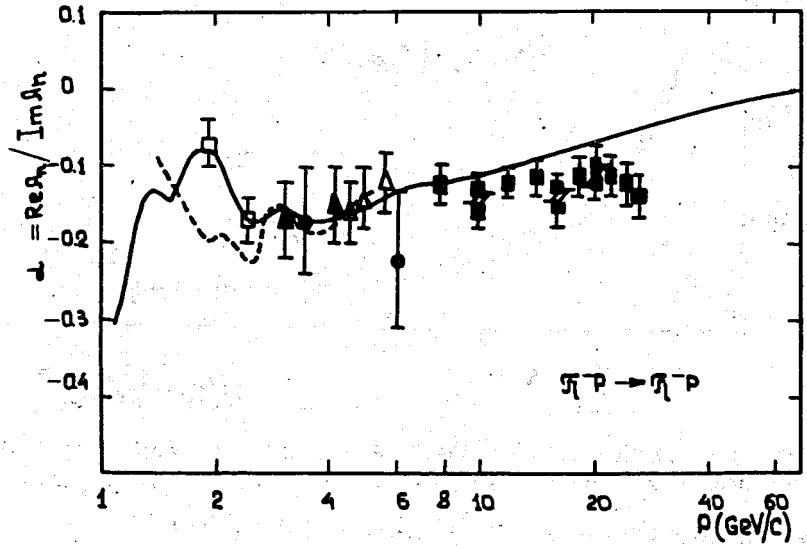

Fig. 10. $\alpha = \mathrm{Re}A_n/\mathrm{Im}A_n$ as a function of the incident particle momentum for $\pi^- p \to \pi^- p$ at $t \to 0$. Experimental dots: △ data of ref. /3,4/; ▲ data of ref. /1/; ● data of ref. /16/; □ data of this paper; ■ data of ref. /6/; Theoretical cirves: —— from ref. /7/; --- from ref. /8/.